Comparison of the photoluminescence properties of semiconductor quantum dots and non-blinking diamond nanoparticles. Observation of the diffusion of diamond nanoparticles in living cells

Orestis Faklaris   Laboratoire de Photonique Quantique et Moléculaire, Ecole Normale Supérieure de Cachan, UMR CNRS 8537, Cachan, France

Damien Garrot   Laboratoire de Photonique Quantique et Moléculaire, Ecole Normale Supérieure de Cachan, UMR CNRS 8537, Cachan, France

Vandana Joshi   Laboratoire Structure et Activité des Biomolécules Normales et Pathologiques, Université Evry-Val-d'Essonne and INSERM U829, Evry, France

Jean-Paul Boudou   Laboratoire Structure et Activité des Biomolécules Normales et Pathologiques, Université Evry-Val-d'Essonne and INSERM U829, Evry, France

Thierry Sauvage   Laboratoire CEMHTI (Conditions Extrêmes et Matériaux : Haute Température et Irradiation), UPR CNRS 3079, Orléans, France

Patrick A. Curmi   Laboratoire Structure et Activité des Biomolécules Normales et Pathologiques, Université Evry-Val-d'Essonne and INSERM U829, Evry, France

François Treussart   Laboratoire de Photonique Quantique et Moléculaire, Ecole Normale Supérieure de Cachan, UMR francois.treussart@ens-cachan.fr   CNRS 8537, Cachan, France

Long-term observations of photoluminescence at the single-molecule level were until recently very difficult, due to the photobleaching of organic fluorophore molecules. Although inorganic semiconductor nanocrystals can overcome this difficulty showing very low photo-bleaching yield, they suffer from photoblinking. A new marker has been recently introduced, relying on diamond nanoparticles containing photoluminescent color centers. In this work we compare the photoluminescence of single quantum dots (QDs) to the one of nanodiamonds containing a single-color center. Contrary to other markers, photoluminescent nanodiamonds present a perfect photostability and no photoblinking. At saturation of their excitation, nanodiamonds photoluminescence intensity with a single NV-color center is only three times smaller than one of the single QDs. Moreover, the bright and stable photoluminescence of nanodiamonds allows wide field observations of single nanoparticles motion. We demonstrate the possibility of recording the trajectory of such single particle in culture cells. [DOI: 10.2971/jeos.2009.09035]

Keywords: quantum dots, nanodiamonds, biomarker, photoluminescence, photostability

1 INTRODUCTION

An important requirement to understand biomolecules interactions is to be able to probe each of them individually at the single molecule scale. For this purpose a stable and reliable marker is needed. Contrary to organic dyes and fluorophores that are widely used but photobleach after some time of illumination, semiconductor nanocrystals (or QDs) have a low photobleaching yield [1]. In addition, QDs offer the possibility of multicolor staining by size tuning. However they may be cytotoxic on long-term scale [2] and they present the important drawback of showing intermittency in their emission, also known as photoblinking [3].

In contrast photoluminescent nanodiamonds (PNDs) are promising alternative biomarkers. Their photoluminescence results from embedded nitrogen-vacancy color centers (NV) [4] in the diamond matrix, which present perfect photostability : no photobleaching, nor photoblinking. Such remarkable properties allow reliable single particle tracking [5, 6]. The low cytotoxicity of nanodiamonds produced by High Pression and High Temperature (HPHT) [7, 8]

and of nanodiamonds produced by detonation [9, 10] has also been demonstrated. In addition PNDs are internalized spontaneously in different cell lines, either by endocytosis or by other mechanisms [8]. These advantages give to PNDs the potential of multiple applications in biology, for example as a marker of different intra or extra cellular compartments or as a long term traceable delivery vehicle for biomolecules translocation in cell.

In this work, we compare the photoluminescent properties of QDs and PNDs. We selected QDs as a reference because they are widely used and have the best photoluminescent properties among inorganic biomarkers. The photoluminescence properties of individual nanoparticles of both types were studied with a home-made confocal microscope equipped with single photon detectors, a time correlation measurement setup and an imaging spectrograph.

Interestingly we observed the photoblinking of QDs and showed that, on the contrary, the PNDs photoluminescence
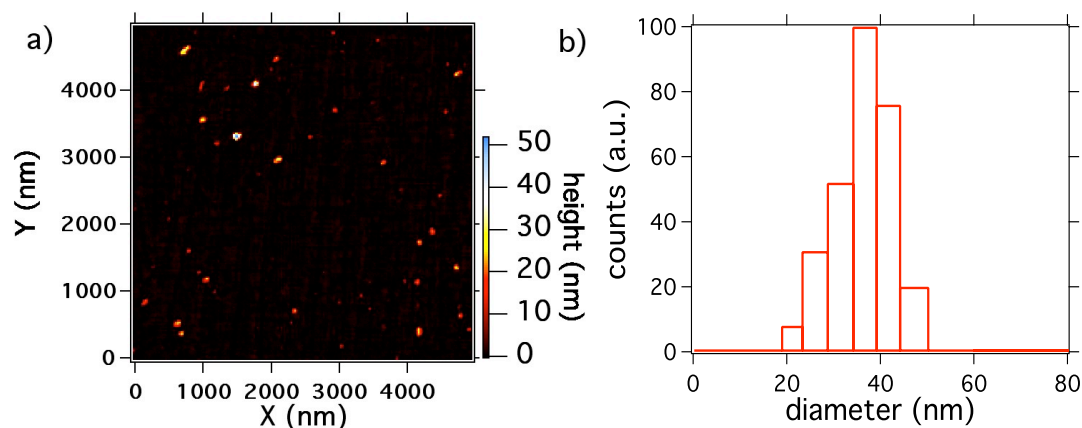
FIG. 1 Size distribution of the PDNs (initial nanodiamond size < 50 nm) redispersed in the aqueous solution: a) Atomic Force Microscope scan of PNDs deposited on a mica plate (apparatus: *Nanoscope IIIa*, Veeco Instruments Inc., USA). b) Dynamic Light Scattering measurement of PNDs in the aqueous solution (apparatus: *BI-200SM*, Brookhaven Instruments Corp., USA).

remains stable in time. We compared the photoluminescence intensity of single QDs with the one of single NV emitters and found only a three fold ratio in favor of QDs. In addition, we studied internalized PNDs in living cells in culture, using wide field laser illumination microscopy. PNDs trajectories were recorded with a standard cooled CCD array. We observed a confined motion of these particles inside the cell cytoplasm, contrary to their free brownian motion measured independently in water:glycerol mixture used as a calibration medium. Such measurements show that the PNDs can be considered as reliable long-term markers for intracellular studies.

2 EXPERIMENTAL METHODS

2.1 Quantum dots and photoluminescent nanodiamonds preparation

The Quantum Dots used are Qdot655-IgG conjugates (*lot N° 51017A*, Invitrogen, USA). They are CdSe core QDs, with a shell of ZnS. This specific QD reference was chosen because its photoluminescence emission peak is centered on 655 nm (Figure 2(b)), close to the NV color center emission spectrum maximum (Figure 4(b)). The diamond nanoparticles are turned into PNDs following the procedure described in [11]. The starting material is synthetic type Ib diamond powder (*SYP 0-0.05*, Van Moppes, Switzerland) with a specified size smaller than 50 nm. The creation of the vacancies is performed by high energy proton irradiation (Van de Graaff accelerator; dose: 5×10^{15} H^+/cm^2, energy: 2.6 MeV) of nanodiamonds and their stabilization next to a nitrogen impurity (forming the stable complex NV) results from subsequent annealing ($800°C$, under inert gas, for 2 hours). For the irradiation process the nanodiamonds were deposited on a silicon wafer as compact thin layers of thickness smaller than 30 μm, to ensure a uniform spatial distribution of the vacancies created by the ion beam in the diamond matrices, as predicted by SRIM Monte Carlo simulations. After these physical processes, the deagglomeration of the nanodiamonds is achieved by strong acid treatment (H_2SO_4:HNO_3, 1:1 vol:vol, at $75°C$ for 3 days) and 2 to 3 times rinsing by deionized water, to finally obtain a stable aqueous suspension. The zeta potential of this solution

was -41.3 mV (apparatus: *Zetasizer Nano ZS*, Malvern, England), a high value probably due to the abundance of acidic groups on the nanodiamond surface, consecutive to the strong acid treatment [7]. The PNDs size distribution, measured after their whole preparation process, yields a mean value of 41 nm (calculated by AFM and DLS, Figure 1), proving that we were able to redisperse the nanodiamonds to their primary size (initial mean size 35 nm). By repeated centrifugations, we can further select an ensemble of smaller PNDs from this suspension.

2.2 Confocal imaging of QDs and PNDs

The QDs and PNDs are deposited on the glass substrates by spin-coating. The photoluminescence of the QDs and the PNDs is studied with a home-made scanning stage confocal microscope (see *Supplementary File* for its detailed description). We use a cw excitation laser at a wavelength of 532 nm well adapted to the QD and NV center [12] absorption spectra. The number of NV color centers per diamond nanoparticle is measured using photon antibunching experiments, relying on a Hanbury Brown and Twiss time intensity correlator [11, 13].

2.3 Wide-field imaging and cells preparation

The experimental setup was the same as the one used for confocal imaging, with two modifications. First, the excitation 532 nm laser beam was defocused before entering the objective of the microscope by a 300 mm lens, making the beam converge onto the back focal plane of the objective. Secondly, the side output port of the microscope stand was used to image the focal plane onto a sensitive CCD array (*CoolSnap Monochrome*, Photometrics, USA).

HeLa cells were grown in standard conditions on glass coverslips in Dulbecco's Modified Eagle Medium (DMEM), supplemented with 10% Foetal Calf Serum (FCS). To study the internalization of PNDs, cells were seeded at a density of 10^5 cells/1.3 cm^2 and grown at $37°C$ in a humidified incubator under 5% CO_2 atmosphere. Twenty-four hours after the cell seeding, the PNDs aqueous suspensions were added to
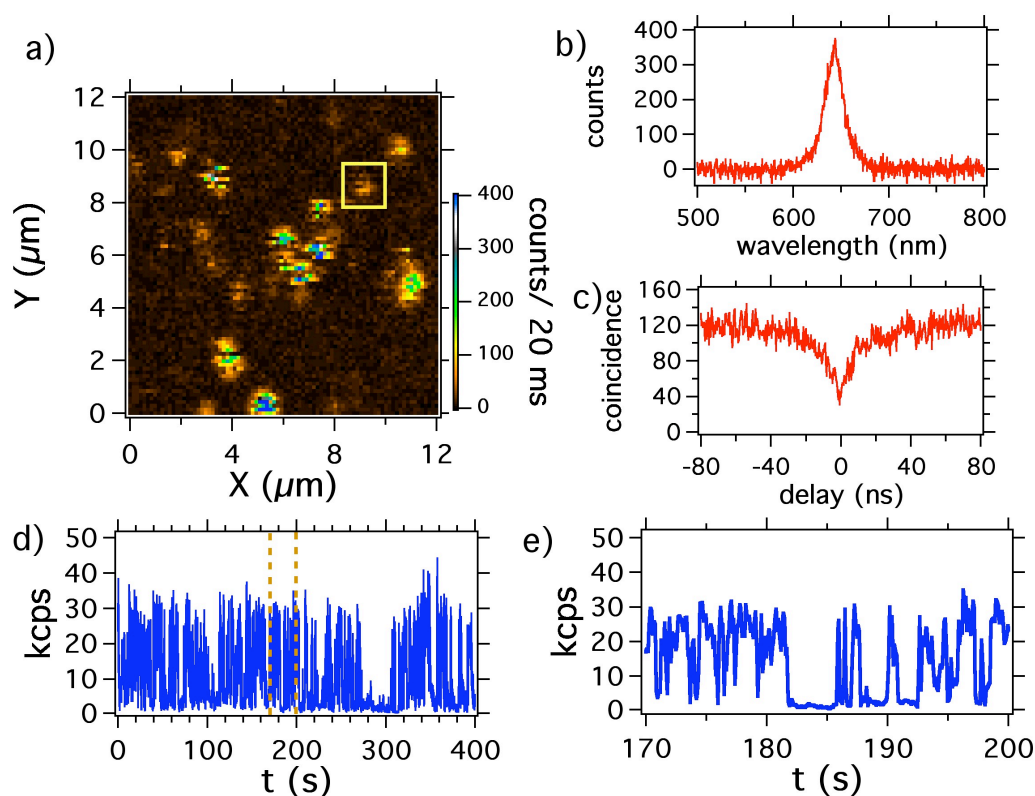
FIG. 2 Photoluminescence intensity of single QDs showing photoblinking. The cw excitation laser used has a wavelength of 532 nm. a) Confocal raster scan of a sample made of QDs spincoated on a glass coverslip, laser excitation power: 5 μW; the blinking of QDs during the scan acquisition can be observed as dark lines interrupting bright spots. b) Photoluminescence spectrum of the QD surrounded with a yellow square on the raster scan a). c) Intensity time correlation histogram of the same QD, showing antibunching at zero delay which proves that we address a single emitter; d) A 400 s long photoluminescence intensity trajectory of the same single QD (binning: 100 ms), laser excitation power: 10 μW; e) zoom of the photoluminescence time-trace of d).

the cell medium. We performed the microscope observations after two hours incubation of the cells with the PNDs .

3 RESULTS AND DISCUSSION

In the following, we compare the saturation behavior of the photoluminescence signals from single QDs and single PNDs, upon increase of the laser excitation power. We study few emitters of each type and we then extract a mean behavior. The excitation laser beam is therefore polarized circularly to be insensitive to the different single-emitter dipole orientations, which could have led to some artifact.

3.1 Photoluminescence study of single quantum dots

Figure 2(a) shows a confocal raster scan of QDs deposited on a glass coverslide. Most of the isolated spots are well separated from each other except one aggregate in the center of the image. The characteristic peak around 655 nm in the photoluminescence spectrum from a single spot allows us to confirm that the emission comes from a QD. The intensity time-correlation measurement of the light emitted from each isolated spot yields a photon antibunching corresponding to a single QD. To study the single-particle photoluminescence, we record the intensity during a "long" integration time of 400 s. We clearly observe blinking in the photoluminescence,

corresponding to the emitter switching randomly between an "on" and an "off" state (Figure 2(d)).

Considering the large fluctuations of the QDs photoluminescence intensity due to this blinking, defining a photoluminescent intensity is somewhat arbitrary (see Figure 2(e), for example) and depends on whether we consider that the emission obeys a simple two states "on"-"off" model, or rather a three-state or even a continuous-state model [14, 15]. In most of the reported works the methods that are used to quantify the photoluminescence intensity signal introduce a threshold level below which the QDs are considered to be in the "off" state. Despite the fact that more complicated techniques have recently been developed, like the changepoint method [16], we decided to use a threshold limit and set it at 50% of the maximum photoluminescence intensity observed on the time window of the measurement.

Figure 3(a) shows the photoluminescence intensity vs the laser excitation power for a single QD. Most of the QDs studied show a decrease of their photoluminescence intensity at a high excitation power, which almost vanishes at intensities higher than 50 kW/cm^2 (corresponding to 100 μW input power). We tentatively attribute this effect to photoinduced oxidation of the QDs surface. The photoluminescence saturation behavior is recorded for 5 single QDs from which an average curve is inferred (see Figure 3(b)). The later indicates that the saturation is achieved for 20 μW excitation power
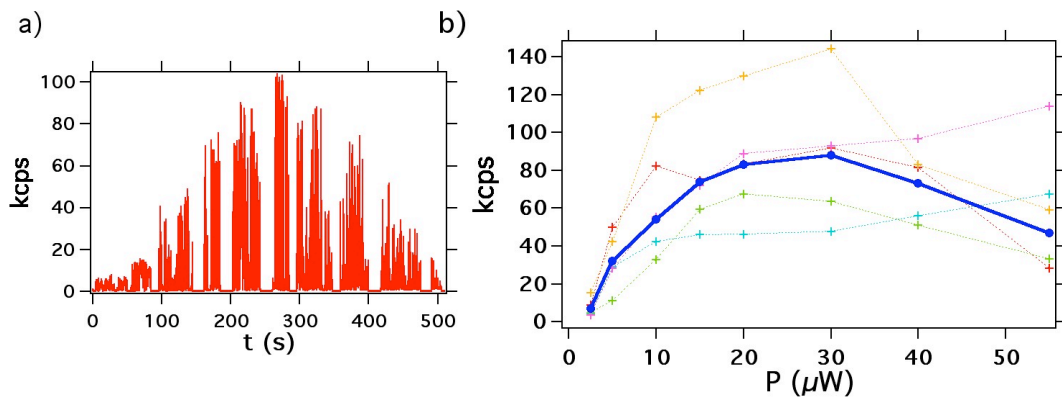
FIG. 3 Photoluminescence intensity vs laser excitation power for QDs. a) Single QD photoluminescence intensity dependence with excitation power, consecutive values equal to 2.5 μW, 5 μW, 10 μW, 12 μW, 15 μW, 20 μW, 30 μW, 40 μW, 55 μW and 100 μW. For every change of the excitation laser power, we shut off the excitation beam for a few seconds in order to measure exactly its the power value; binning time: 50 ms. b) Mean saturation curve (plain blue) calculated from the average of 5 single QDs saturation curves (dashed colored).
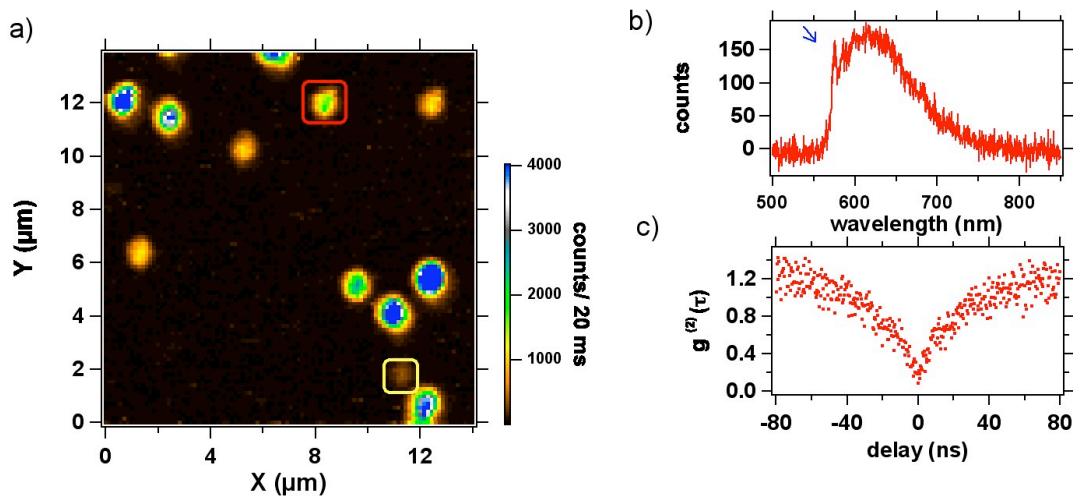

FIG. 4 Photoluminescence of a single PND : a) Confocal raster scan, excitation laser power: 1 mW; the well isolated spots correspond to PNDs. b) Photoluminescence spectrum of the PND surrounded in yellow (bottom right angle), corresponding to the emission of a neutral NV^0 color center, identified thanks to its narrow Zero Phonon Line (ZPL, blue arrow) at 575 nm. c) Intensity time-correlation function $g^{(2)}$ of the same PND, showing photon antibunching at zero delay, associated to the emission of single photons. This observation proves that we address a single color center.

corresponding to a maximum photoluminescence intensity of 82 kcounts/s (kcps). This value is compared with the one found for PNDs in the following. Note that the counting rates considered here correspond to photoluminescence intensity records of one of the two avalanche photodiodes only, i.e. on one side of the Hanbury-Brown and Twiss correlation setup. They are roughly equal to half of the total counting rate.

3.2 Photoluminescence study of single NV color centers in nanodiamonds

3.2.1 Results

In order to compare the photoluminescence of QDs with that of PNDs we performed similar saturation measurements for single NV color centers in the diamond nanocrystals of mean size 41 nm. Figure 4(a) shows a confocal raster scan of PNDs deposited on a glass coverslip. The photoluminescence spots observed have emission intensities varying a lot from one spot to the other. This is due to an inhomogeneous number of NV centers per nanocrystal. We selected a nanocrystal containing

a single NV center (assessed by Figure 4(c) antibunching measurement) and we recorded its saturation curve. The saturation occurs for excitation power value higher than 1.5 mW, corresponding to a photoluminescence intensity of 25 kcps. Note that compared to QDs, the NV photoluminescence intensity is constant in time (Figure 5(a)). The Signal-to-Noise Ratio (SNR) for this PND is about 10 (ratio of $\langle N \rangle = 380$ to the standard deviation $\sigma = 37$), while the shot-noise-limited SNR is by definition $\sqrt{N} \approx 19.5$. This excess of noise can be explained by a bunching effect in the photon stream that shows up as a $g^{(2)}(\tau)$ greater than 1 (Figure 4(c)).

3.2.2 Discussion

According to our measurements, a single QD yields an emission intensity at saturation three times larger than the one of a single NV center. In addition the excitation laser saturation power for a single QD is $\times 75$ lower than the one required for a NV center. This result can be explained by the difference in the absorption cross section σ of the two type of emitters.
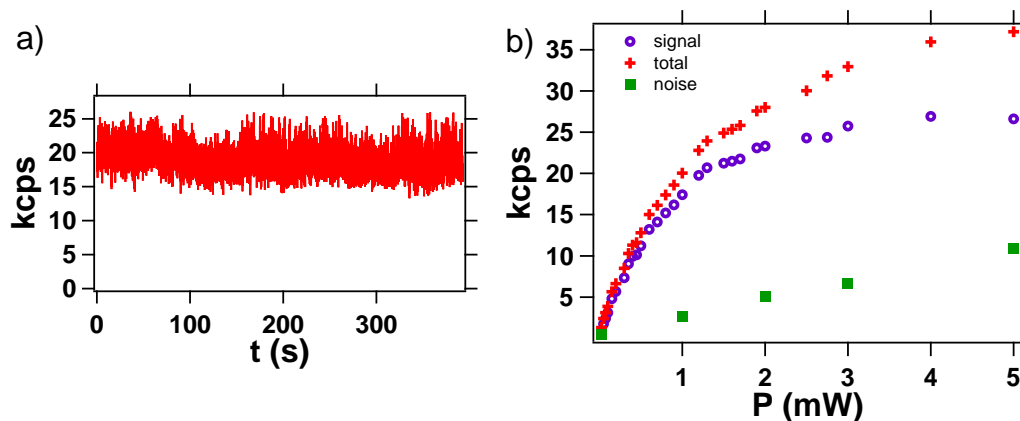
FIG. 5 Photoluminescence intensity stability and saturation curve for a single NV color center in a PND : a) Photoluminescence signal (binning 20 ms) recorded over a time duration of 395 s, showing the perfect photostability of NV center emission. b) Photoluminescence intensity curve vs laser excitation power, for the single NV center surrounded in yellow in Figure 4(a). Green squares correspond to the background coming from the substrate and recorded from a position a few hundreds of nanometers next to the PND; red crosses are associated to the total signal collected from the PND location; purple circles is the signal corrected from the background.

The absorption cross-section was inferred in the range $\sigma_{QD} \approx 2 - 16 \times 10^{-16}$ cm^2 [17] at 488 nm excitation wavelength for the QD, while for the NV center $\sigma_{NV} \approx 3 \times 10^{-17}$ cm^2 [18]. Considering that the excitation intensity at saturation is proportional to $(\sigma\tau)^{-1}$ (τ being the emitter radiative lifetime), and taking into account that the QD and the NV color center have similar lifetime $\tau \approx 20$ ns, the change in the saturation intensity results only from the change in the absorption cross-sections. A maximal value of $\sigma_{QD}^{max}/\sigma_{NV} = 54$ is then expected, which is slightly lower than the one observed experimentally. This discrepancy may be due to the very small number of emitters studied which leads to non statistically significant measurements.

Regarding the stability of the photoluminescence intensity in time, the QDs clearly show intermittent emission while the NV centers photoluminescence intensity is perfectly stable. Recent studies show that the QD core-shell can be optimized to reduce the blinking [19, 20]. But despite the progress in suppressing the photoblinking, a significant fraction of the QDs nanocrystals still blinks. Moreover, the blinking properties depend on the excitation power and obey to non-classical statistics [21].

Even though the photoluminescence intensity from a single NV center is three times smaller than the one from a QD, if we consider their perfect photostability they are still very interesting markers for applications in biology. In addition, by selecting nanodiamonds rich in nitrogen (nitrogen concentrations larger than 100 ppm) and by optimizing the conditions for the NV color center creation (irradiation and annealing process), we managed to obtain nanocrystals of about 40 nm in size, containing up to 4-5 NV centers. On the Figure 4(a) raster scan, the spot circled in red corresponds to a nanocrystal containing 5 NV centers. Such a nanocrystal displays a higher photoluminescence intensity than the one of a single QD of similar size. Moreover, the irradiation dose used to create the vacancies in the PNDs can still be increased by at least one order of magnitude, using the same accelerator. Therefore, we should be able to produce even brighter PNDs.

3.3 Wide-field microscopy observations of freely diffusing PNDs

For biological applications wide-field microscopy is of great importance. In such experiments, QDs have already been used as biomarkers to study the dynamics of biomolecules [22, 23]. However due to their blinking, the tracking of a single QD appears to be tedious, which strongly limits its use in such applications. In comparison, a PND containing many NV centers can be as bright as a QD, with the additional property of a perfectly stable emission, well suited for tracking over a long observation period.

In order to prove this statement, we first examined the free brownian motion of PNDs in solution. We used PNDs of two different sizes, the previously mentioned 41 nm and other ones of size 163 nm, as measured by dynamic light scattering (Figure S2 of the *Supplementary File*). Figure 6(a) is associated to the video of 163 nm in size PNDs, freely diffusing in a 20% water - 80% glycerol solution. The PNDs diffusion in this solution is a free 3D-brownian motion, but the observations are restricted to the portion of this motion taking place in the focus plane. More precisely only PNDs which are moving within a slice of thickness equal to the depth of focus ($\approx$ 810 nm) are observed. Therefore the motion recorded is a 2D-projection of *portions* of the 3D trajectory contained in this slice. To construct the particles trajectory from this record, we used the "ParticleTracker" plugin of NIH-*ImageJ* software, which implements the algorithm of Ref. [24]. The particles that are too far from the middle plane of the focusing slice appear as non diffraction-limited dimmer spots that are excluded with the software, using a filtering procedure. This procedure relies on a size restriction and intensity level cutoff. It filters the particles motions which take place in a slice thinner than the one limited by the optical depth of focus, so that the motion really taken into account for the trajectory construction is very close to a 2D one.

The "ParticleTracker" plugin also constructs a trajectory with a step resolution better than the real-space pixel size of $\approx$ 140 nm. To do so, it extracts the PND position in each frame
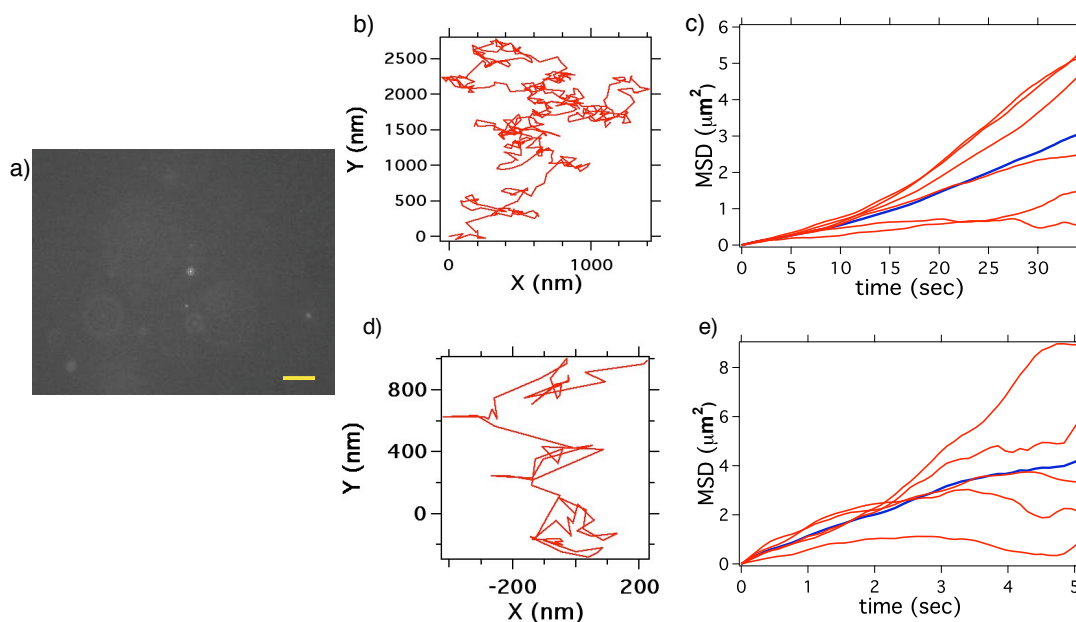
FIG. 6 Free brownian diffusion of PNDs in a water:glycerol mixture : a) Video sequence of 163 nm PNDs diffusing in a 20% water - 80% glycerol solution; exposure time per frame: 100 ms; this relatively long integration time is not a problem in our study as the water-glycerol proportion was deliberately chosen to have slow nanodiamonds motions, allowing the resolution of individual steps in time; scale bar: 5 μm. b) Trajectory of a single PND executing a free brownian motion. c) Mean square displacements (MSD) for six different PNDs; the blue line is the mean value; d-e) similar to b-c) but for 41 nm mean size PNDs. (size 2 MB, format: mov, see Fig6a.mov)

from the maximum of a gaussian fit of the single emitter spot (which covers about 4 pixels). The program uses a discretization step of 23 nm which is 6 times smaller than the pixel size. This procedure allows us to infer displacements smaller than the pixel size. The noise on the localization of a spot was also estimated of the order of 25-30 nm from measurements done on fixed PNDs embedded in a polymer layer. We provide in the *Supplementary File* the example of a PND trajectory inside the same cell (Figure S3c) showing a directed motion on a short distance, with a lateral spatial broadening of the same 25-30 nm order of magnitude. This observation confirms the static noise measurements.

After the video processing, and the trajectory reconstruction, the PNDs were mostly found to follow brownian trajectories with no directional force. A usual method to provide a diffusion coefficient is to calculate the mean square displacements (MSD) [25]. For spherical particles executing a 2D free brownian motion, $MSD(t) = 4Dt$, where D is the diffusion coefficient and t the diffusion time. In case there are external forces (drifts) acting on the particles, the equation becomes $MSD(t) = 4Dt + v^2(t)$, where v represents the velocity of the directional movement [26]. For the PNDs of size 163 nm, the diffusion coefficient measured $D = 0.04$ $\mu m^2/s$. This is the mean value out of 6 particles, with lower and higher value at $D = 0.01$ $\mu m^2/s$ and $D = 0.05$ $\mu m^2/s$ respectively. A lower bound to the error bars then results from this two extreme slopes of the $MSD(t)$. We repeat the experiment for the 41 nm mean size PNDs (Figure 6(d)-(f)). The diffusion coefficient measured is equal to $D = 0.20$ $\mu m^2/s$, which is 5 times bigger than the one of 163 nm PNDs. This measurement is the mean value over 5 particle trajectories, with extremes at $D = 0.05$ $\mu m^2/s$ and $D = 0.35$ $\mu m^2/s$ as lower and higher value respectively.

The above experimental values can be compared to the theoretical predictions given by the Stokes-Einstein equation $D = kT/(6\pi\eta a)$, a being the particle radius, η the viscosity of the medium (60 cP in our case), k the Boltzman constant, and T the temperature. The diffusion coefficients for 41 and 163 nm particles inferred from this equation are equal to $D = 0.18$ $\mu m^2/s$ and $D = 0.04$ $\mu m^2/s$ respectively. These values agree well with the experimental ones.

Note that the error bars on the measurement of the diffusion coefficients are large, which is an observation already reported in previous studies [26]. This broad distribution is mainly due to the fact that the trajectory analysis is done on a too small number of steps. The precision on the measurement of D improves with the increase of the statistical sampling of the trajectory. However in a 2D study, it is not easy to record a continuous trajectory over a long observation time, since the particles, especially the small ones, are out of focus as soon as they are moving along the z axis perpendicular to the focus plane. In addition, one other reason for a broad distribution of the diffusion coefficient is the particle size distribution, which is itself also very broad (see Figure S2 of *Supplementary File*).

3.4 Diffusion of PNDs in living cells

The tracking of individual biomolecules in cells is of great importance in biology. In case the biomolecule is not photoluminescent, a photoluminescent marker can be attached to it so as to follow its motion. If we want to use PNDs as markers, the first step is to verify that such particle can enter the cell which was the topic of a previous work [8] and then to follow its trajectory in time.

Figure 7(a) shows the video sequence of real-time motions of 41 nm PNDs in cell. It is clear that the motion is much
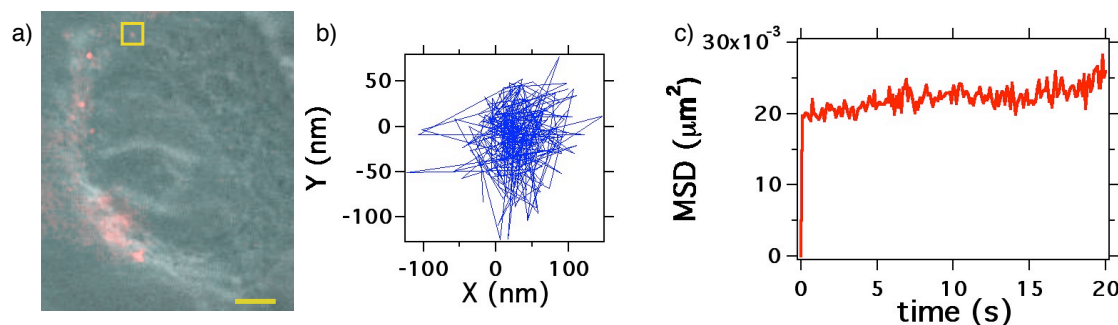
FIG. 7 Intracellular trafficking of single 41 nm PNDs in a live HeLa cell : a) Phase contrast image of the cell (centered on the cell nucleus) merged with fluorescence image of PNDs (in red); bar scale: 3 μm. The real-time video sequence of PNDs in the cell associated to image a) is recorded with an acquisition time per frame of 100 ms. b) Trajectory of the PND located inside the yellow square. c) Mean square displacement of this PND. (size 172 kB, format: mov, see Fig7a.mov)

more confined than in the glycerol-water solution. Note that the confinement dimension is about 160 nm, a value of about one order of magnitude larger than the noise limit. This result proves that we observed a true -although very small- motion of the PND. By analyzing the MSD values at short times [27] we determine an equivalent "diffusion coefficient" $D = 0.006 \; \mu m^2/s$, and among all the particle motion studied, the maximum diffusion coefficient found does not exceed the value of 0.01 $\mu m^2/s$, in agreement with previous calculations [5]. The reason for the PNDs low mobility in cells is that the observed PNDs are probably captured in endosomal or lysosomal vesicles [8].

4 CONCLUSION

In conclusion, we showed that in terms of photoluminescence, 41 nm PNDs can be as bright as QDs, even brighter when they contain more than 4-5 NV color centers. Contrary to QDs, their emission is perfectly stable in time. An application of such PNDs with many NV centers in their matrix is the single biomolecule tracking. As a proof of concept, we first showed that the free diffusion of single PNDs of different size can be recorded in wide field microscopy using a standard cooled CCD array detector. We further incubated PNDs with cells and observed the motion of the internalized PNDs, that appears to be confined probably in cell compartments. Our results indicate that PNDs can be used for long-term single particle tracking, and have therefore the potential of being reliable biomarkers.

References

[1] X. Michalet, F. F. Pinaud, L. A. Bentolila, J. M. Tsay, S. Doose, J. J. Li, G. Sundaresan, A. M. Wu, S. S. Gambhir, and S. Weiss, "Quantum Dots for Live Cells and in vivo Imaging, Diagnostics and Beyond" Science **307**, 538–544 (2005).

[2] C. Kirchner, T. Liedl, S. Kudera, T. Pellegrino, A. M. Javier, H. E. Gaub, S. Stolzle, N. Fertig, and W. Parak, "Cytotoxicity of colloidal CdSe and CdSe/ZnS nanoparticles" Nano Lett. **5**, 331–338 (2005).

[3] M. Nirmal, B. Dabbousi, M.G. Bawendi, J. J. Macklin, J. K. Trautman, T. D. Harris,and L. E. Brus, "Fluorescence intermittency in single cadmium selenide nanocrystal" Nature **383**, 802–804 (1996).

[4] A. Gruber, A. Dräbenstedt, C. Tietz, L. Fleury, J. Wrachtrup, and C. von Borczyskowsky, "Scaning confocal optical microscopy and magnetic resonance on single defect centers" Science **276**, 2012–2014 (1997).

[5] F. Neugart, A. Zappe, F. Jelezko, C. Tietz, J.P. Boudou, A. Krueger, and J. Wrachtrup, "Dynamics of diamond nanoparticles in solution and cells" Nano Lett. **7**, 3588–3591 (2007).

[6] Y.-R. Chang, H.-Y. Lee, K. Chen, C.-C. Chang, D.-S. Tsai, C.-C. Fu, T.-S. Lim, Y.-K. Tzeng, C.-Y. Fang, C.-C. Han, H.-C. Chang, and W. Fann, "Mass production and dynamic imaging of fluorescent nanodiamonds" Nat. Nanotechnol. **3**, 284–288 (2008).

[7] C.-C. Fu, H. Y. Lee, K. Chen, T.-S. Lim, H.-Y. Wu, P.-K. Lin, P.-K. Wei, P.-H. Tsao, H.-C. Chang, and W. Fann, "Characterization and application of single fluorescent nanodiamonds as cellular biomarkers" Proc. Natl. Acad. Sci. U.S.A. **104**, 727–732 (2007).

[8] O. Faklaris, D. Garrot, V. Joshi, F. Druon, J.P. Boudou, T. Sauvage, P. Georges, P. Curmi, and F. Treussart, "Detection of single photoluminescent diamond nanoparticles in cell and study of the internalization pathway" Small **4**, 2236–2239 (2008).

[9] A. M. Schrand, H. J. Huang, C. Carlson, J. J. Schlager, E. Osawa, S. M. Hussain, and L. Dai, "Are diamond nanoparticles cytotoxic?" J. Phys. Chem. B **16**, 2118–2123 (2007).

[10] H. Huang, E. Pierstorff, E. Osawa, and E. Ho, "Active nanodiamond hydrogels for chemotherapeutic delivery" Nano Lett. **1**, 3305–3314 (2007).

[11] Y. Sonnefraud, A. Cuche, O. Faklaris, J.P. Boudou, T. Sauvage, J. F. Roch, F. Treussart, and S. Huant, "Diamond nanocrystals hosting single nitrogen-vacancy color centers sorted by photon-correlation near-field microscopy" Opt. Lett. **33**, 611–613 (2008).

[12] Y. Mita, "Change of absorption spectra in type Ib diamond with heavy neutron iradiation" Phys. Rev. B **53**, 11360–11364 (1996).

[13] F. Treussart, V. Jacques, E. Wu, T. Gacoin, P. Grangier, and J. F.

Roch, "Photoluminescence of single colour defects in 50 nm diamond nanocrystals" Physica B **376**, 926–929 (2006).

[14] R. Verberk, A. M. van Oijen, and M. Orrit, "Simple model for the power-law bliking of single semiconductor nanocrystals" Phys. Rev. B **66**, 233202 (2002).

[15] K. Zhang, H. Chang, A. Fu, P. Alivisatos, and H. Yang, "Continuous distribution of emission states from single CdSe/ZnS Quantum Dots" Nano Lett. **6**, 843–847 (2006).

[16] L. P. Watkins, and H. Yang, "Detection of intensity change points in time-resolved Single-Molecule measurement" J. Phys. Chem. B **109**, 617–628 (2004).

[17] B. Lounis, H. A. Bechtel, D. Gerion, P. Alivisatos, and W. E. Moerner, "Photon antibunching in single CdSe/ZnS quantum dot fluorescence" Chem. Phys. Lett. **329**, 399–404 (2000).

[18] T. L. Wee, Y.-K. Tzeng, C.-C. Han, H.-C. Chang, W. Fann, J.-H. Hsu, K.-M. Chen, and Y.-C. Yu, "Two-photon excited fluorescence of nitrogen-vacancy centers in proton-irradiated type 1b diamond" J. Phys. Chem. A **100**, 9379-9386 (2007).

[19] B. Mahler, P. Spinicelli, S. Buil, X. Quelin, J. P. Hermier, and B. Dubertret, "Towards non-blinking colloidal quantum dots" Nat. Nanotechnol. **7**, 659–664 (2008).

[20] Y. Chen, J. Vela, H. Htoon, J. L. Casson, D. J. Werder, D. A. Bussian, V. I. Klimov, and J. A. Hollingsworth, "Giant multishell CdSe nanocrystal Quantum Dots in suppressed blinking"J. Am. Chem. Soc. **130**, 5026–5027 (2008).

[21] P. Didier, L. Guidoni, and F. Bardou, "Infinite average lifetime of an unstable bright state in the green fluorescent protein" Phys. Rev. Lett. **95**, 090602/1–4 (2005).

[22] M. Dahan, S. Levi, C. Luccardini, P. Rostaing, B. Riveau, and A. Triller, "Diffusion dynamics of glycine receptors revealed by single-quantum dot tracking" Science **302**, 442–445 (2003).

[23] L. Groc, M. Lafourcade, M. Heine, M. Renner, V. Racine, J. B. Sibarita, B. Lounis, D. Choquet, and L. Cognet, "Surface trafficking of neurotransmitter receptor: comparison between single-molecule/quantum dot strategies" J. NeuroSc. **27**, 12433 (2007).

[24] I. F. Sbalzarini, and P. Koumoutsakos, "Feature point tracking and trajectory analysis for video imaging in cell biology" J. Struct. Biol. **151**, 182–195 (2005).

[25] M. Saxton, and K. Jakobson, "Single particle tracking: applications to membrane dynamics" An. Rev. Biophys. Biomol. Struct. **26**, 373 (1997).

[26] A. Kusumi, Y. Sako, and M. Yamamoto, "Confined lateral diffusion of membrane receptors as studied by single particle tracking" Biophys. J. **65**, 2021 (1993).

[27] C. Dietrich, B. Yang, T. Fujiwara, A. Kusumi, and K. Jakobson, "Relationship of lipid rafts to transient confinement zones detected by single particles tracking" Biophys. J. **82**, 274 (2002).